David C. Jenn, Phillip E. Pace, and Ric A. Romero

# An Antenna for a Mast-Mounted Low Probability of Intercept Continuous Wave Radar

***Improving performance with digital architecture.***

Continuous wave (CW) low probability of intercept (LPI) radars transmit and receive simultaneously, generally using phased-coded waveforms. This article describes a bistatic radar that uses an omnidirectional transmitting antenna and a receiving array with digitally formed simultaneous overlapping beams for search and track. In addition to coherent leakage cancellation to suppress the transmitter leakage at the receiver, a phase-coding technique is used, allowing the antennas to be closely spaced on a common mast. Both of these capabilities are made possible by the digital architecture of the receiving array.

## THE NEED FOR NEW RADAR FEATURES

Small boats operating in the littoral regions near the shore have a need for a mast-mounted radar to perform search and track functions. The radar's range is inherently limited due to the low mast heights, but high range and velocity resolutions are required. For military operations, covertness is desired. LPI is achieved using a low-power CW phase-coded waveform [1]. The target signal-to-noise ratio (SNR) can be increased by coherent

*Digital Object Identifier 10.1109/MAP.2019.2895666*
*Date of publication: 22 February 2019*


1045-9243/19©2019IEEE

integration, but that requires increasing the target observation time [2]. This leads to large frame times if a single scanning beam is used for 360° azimuth coverage. To avoid long frame times, simultaneous beams are needed.

In a CW radar, transmission and reception must occur simultaneously, so a major challenge is the suppression of leakage from the transmitter to the receiver [3]. Coherent leakage cancellation can be used [3]–[5], but it only provides about 40 dB of reduction, which is not sufficient to unmask small targets on the horizon. This article describes a compact CW radar that employs a digital phased array on receive with two key features that significantly improve the radar performance. First, simultaneous overlapping digital beams provide complete and continuous azimuth coverage. Second, a randomization of the transmitted waveform phase code is used to suppress the transmit–receive leakage, thereby allowing the detection and tracking of distant targets that would normally be lost in the leakage signal. Both of these capabilities are made possible by the digital architecture of the radar system and array.

**Small boats operating in the littoral regions near the shore have a need for a mast-mounted radar to perform search and track functions.**

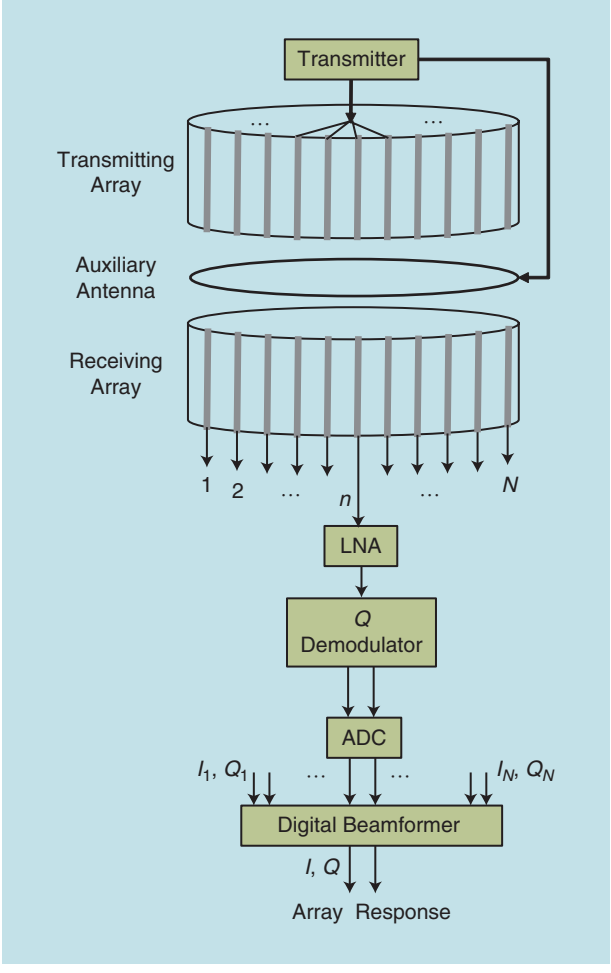


**FIGURE 1.** A simplified radar block diagram showing hardware blocks.

## DESCRIPTION OF THE RADAR AND ANTENNA

The primary radar functions are search and track for situational awareness. For the small craft under consideration, such as rigid-hull inflatable boats, the mast heights are in the range of 2 to 3 m. Only surface targets out to the horizon are of interest. Assuming standard atmospheric conditions, the distance to the horizon for an antenna at 3 m is approximately 7 km [2]. Considering ship motion, an elevation beamwidth of 15 to 20° is acceptable. The radar must provide 360° of azimuth coverage.

The selection of the frequency of operation has a number of important tradeoffs [2]. Aside from the antenna, other radar considerations include clutter characteristics, bandwidth (range resolution), Doppler shift (velocity resolution), and target radar cross section (RCS). A radar installed on the mast would be limited to about 0.3 m in diameter. With regard to the antenna, the lowest frequency is set by the minimum acceptable gain and beamwidth that can be obtained with a 0.3-m-diameter antenna. From a system analysis, the minimum frequency was determined to be in the *X* band. Higher frequencies have the potential for higher gain, but the gain is limited because the antenna elements are located on a cylindrical surface. As will be shown in the section "Receiving Array Digital Beamforming and Antenna Simulations," even with phase corrections added in the digital beamforming, the fact that elements are facing different directions due to the curved surface limits the number of elements that can be used efficiently and, thus, limits the array gain. Another advantage of high operating frequency is the more compact hardware. The results of tradeoff studies indicated that the *K* band was a good compromise, and a frequency of 20 GHz was selected. Based on the radar resolution requirements, a bandwidth of 50 MHz was selected.

A simplified radar system block diagram is shown in Figure 1. Several array element types were considered. H-plane sectoral horns were selected for both the transmitting and receiving arrays because they could be closely spaced and are low loss compared to microstrip elements. The wideband horns (18–26.5 GHz) allow for operating frequency variation and future bandwidth expansion. A radial power divider (i.e., analog beamforming) is used to obtain an omnidirectional transmit pattern in azimuth. H-plane sectoral horns are also used as elements in the receiving array. The output of each horn has a low-noise amplifier and quadrature (*Q*) demodulator, which provides in-phase (*I*) and *Q* outputs. The *I* and *Q* signals are downconverted, sampled with an analog-to-digital converter (ADC), and sent to the signal processor for beamforming and further radar processing. Detailed descriptions of the clutter processing and

integrations to achieve a high processing gain are given in [6].

To relax the ADC requirement, the array outputs are downconverted to an intermediate frequency (IF) less than 200 MHz and then sampled. The IF signals out of the array elements can be transmitted via cables the short distance to the base of the mast with relatively low losses. The IF ADCs and other processing blocks are located at the base, where the packaging volume is not as constrained as it is in the mast. Because transmission is simultaneous with reception, isolation must be maintained. For the scenarios considered, the received echo from a target on the horizon can be at a level of –160 dBW, while the direct leakage from the transmitter to receiver can be as high as –80 dBW, depending on the antenna spacing. An auxiliary antenna is one approach that can be used to increase isolation between the transmitting and receiving horn arrays. This auxiliary antenna provides a cancellation signal to the receiving array that is tuned to subtract signals received directly from the transmitting horns, as discussed in the "Leakage Cancellation and Calibration" section.

**Simultaneous overlapping digital beams provide complete and continuous azimuth coverage.**

## RECEIVING ARRAY DIGITAL BEAMFORMING AND ANTENNA SIMULATIONS

Figure 2 shows the circular array geometry. There are $N$ horn elements depicted by the gray lines. The elements are centered at $(x_n, y_n, 0)$, and their angular positions around the circle of radius $a$ are $\phi_n = \Delta\phi(n-1)$, where $\Delta\phi = 360°/(N+1)$ is the angle increment. The arc-length separation between elements is $s = a(\Delta\phi)$.

The outward normal for element $n$ is given by

$$\hat{r}_n = \hat{x}\cos\phi_n + \hat{y}\sin\phi_n. \quad (1)$$

Using the coordinate system defined in Figure 2, a unit vector in the observation direction is

$$\hat{R} = \hat{x}u + \hat{y}v + \hat{z}w = \hat{x}\sin\theta\cos\phi + \hat{y}\sin\theta\sin\phi + \hat{z}\cos\theta, \quad (2)$$

where $(u, v, w)$ are the direction cosines. Likewise, a unit vector in the scan direction $(\theta_s, \phi_s)$ is

$$\begin{aligned}\hat{R}_s &= \hat{x}u_s + \hat{y}v_s + \hat{z}w_s \\ &= \hat{x}\sin\theta_s\cos\phi_s + \hat{y}\sin\theta_s\sin\phi_s + \hat{z}\cos\theta_s. \end{aligned} \quad (3)$$

Only azimuth scanning is considered, so $\theta_s = 90°$. The receiving beam is obtained by summing the contributions from only the elements with a line of sight (LOS) in the desired scan direction. At most, that would be the half of the elements on the illuminated side of the array, assuming a source in the scan direction. This would be the circles shown in Figure 3, which satisfy

$$\hat{R}_s \cdot \hat{r}_n = \cos(\gamma_n) \geq 0, \quad (4)$$

where $\gamma_n$ is the angle between the element normal and $\hat{R}_s$. However, elements that are rotated significantly from the scan direction, such as those circled in Figure 3, contribute little to the pattern and can be neglected. An advantage of digital beamforming is that elements can be added or removed from the processing to vary the beamwidth and gain depending on the operating conditions.

Let the element amplitude and phase weights be $A_n$ and $\psi_n$, respectively. Due to the elements' pointing in different directions, the element factors must remain inside of the summation when calculating the pattern. From a transmitting perspective, the array pattern is

$$\vec{F}(\theta,\phi) = \sum_{n=N_1}^{N_2} A_n e^{j\psi_n} e^{jk(x_n u + y_n v)} \vec{E}_n(\theta,\phi), \quad (5)$$

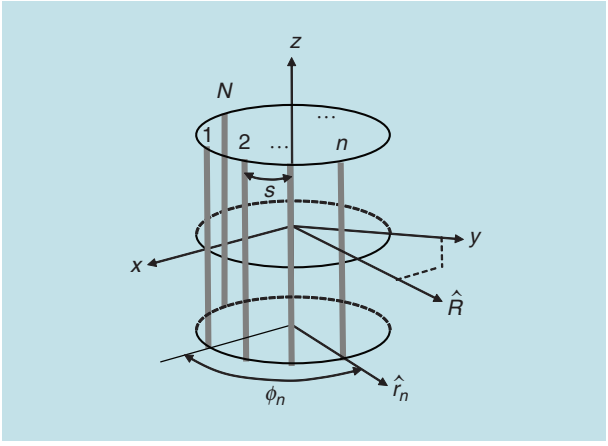


**FIGURE 2.** Cylindrical array geometry of vertical elements.

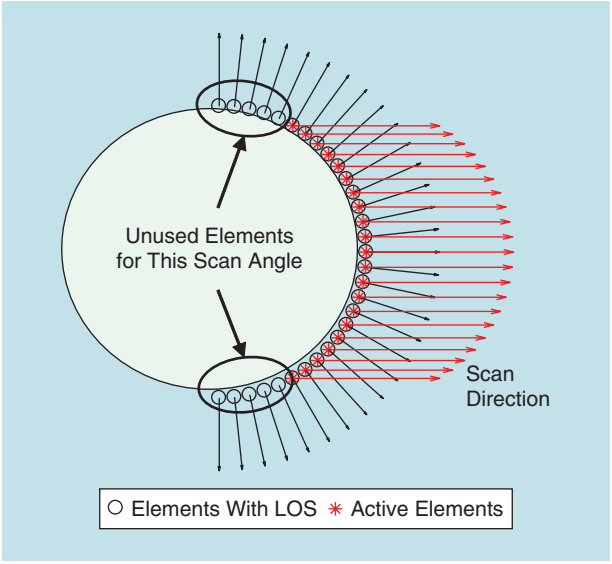


**FIGURE 3.** Limitation of array elements due to their pointing directions.

where $k = 2\pi/\lambda$ ($\lambda$ is the wavelength) and $\vec{E}_n(\theta,\phi)$ is the pattern of element $n$. $N_1$ and $N_2$ are the start and stop indices of the elements used in the beamforming.

The element factor for element $n$ can be approximated by an aperture with a cosine taper ($TE^{10}$ mode). The aperture is defined in a local $(x',y',z')$ coordinate system that is rotated about the global $z$-axis ($\hat{z} = \hat{z}'$). The aperture normal is in the $\hat{x}'$ direction, as shown in Figure 4. The aperture field is polarized as $E_{y'}$ ($E_{z'} = 0$) so that the normalized far field of element $n$ is [7]

$$\vec{E}_n(\theta',\phi') = \sin\theta' \operatorname{sinc}\left(\frac{kbv'}{2}\right) \frac{\cos(kw'A/2)}{1-(kAw'/\pi)^2}\hat{\phi}', \tag{6}$$

where we define $\operatorname{sinc}(\alpha) = \sin(\alpha)/\alpha$. The fields of the individual apertures are transformed back to the global system $E_n(\theta',\phi')\hat{\phi}' \rightarrow E_n(\theta,\phi)\hat{\phi}$ and summed to get the total field from (5).

A focused beam can be obtained by correcting for the array curvature, as shown in Figure 5. The path difference from element $n$ relative to a plane wave at scan angle $\phi_s$ is

$$\psi_n = a[1-\cos(\phi_n - \phi_s)]. \tag{7}$$

The phase correction required to focus is $k\psi_n$. We have ignored mutual coupling, but, because of the circular symmetry, the mutual coupling effects are identical at every element. Mutual coupling is still a consideration in the matching of the array elements.

From a receiving perspective, the $I$ and $Q$ outputs of element $n$ are complex spatial samples of the incident plane wave, including the element factor. The digital array response is formed by weighting and summing the desired outputs:

$$F(\theta,\phi) = \sum_{n=N_1}^{N_2} A_n e^{j\psi_n}(I_n + jQ_n). \tag{8}$$

The directivity of the array (i.e., neglecting losses) can be computed by direct integration of the pattern, which is the same for both transmitting and receiving. The directivity is

$$D = 4\pi/\Omega_A, \tag{9}$$

where

$$\Omega_A = \int_0^{2\pi}\int_0^{\pi} |F_{\text{norm}}|^2 \sin\theta d\theta d\phi \tag{10}$$

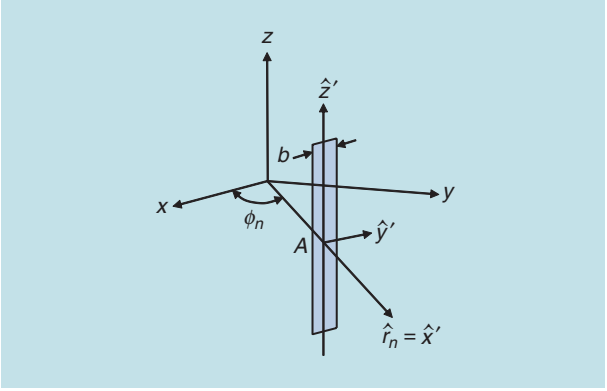


**FIGURE 4.** A rotated slot aperture element with a cosine amplitude taper in $z'$.

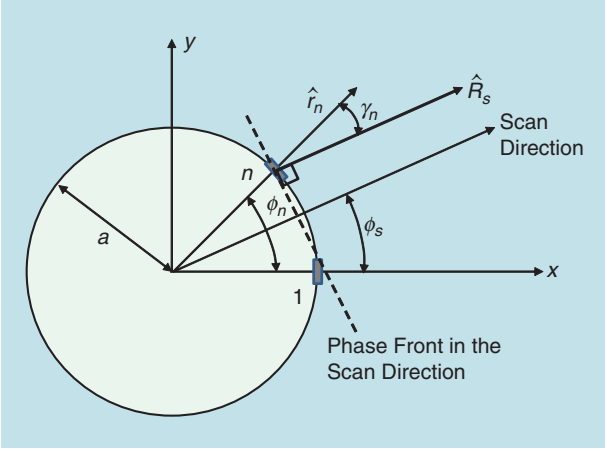


**FIGURE 5.** Correcting for the phase error due to array curvature.

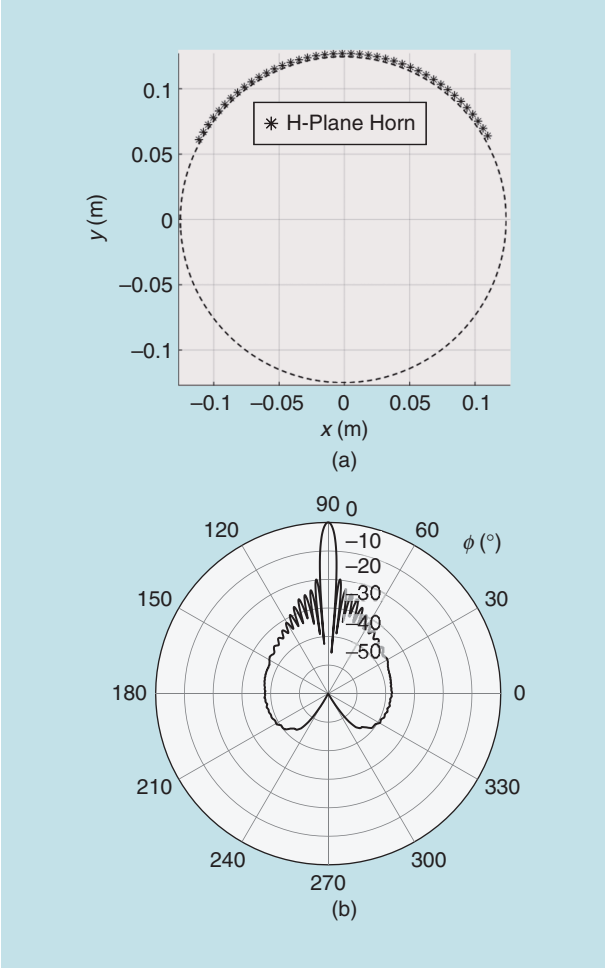


**FIGURE 6.** (a) Elements used to form an azimuth beam at 90° and (b) a radiation pattern at 20 GHz.

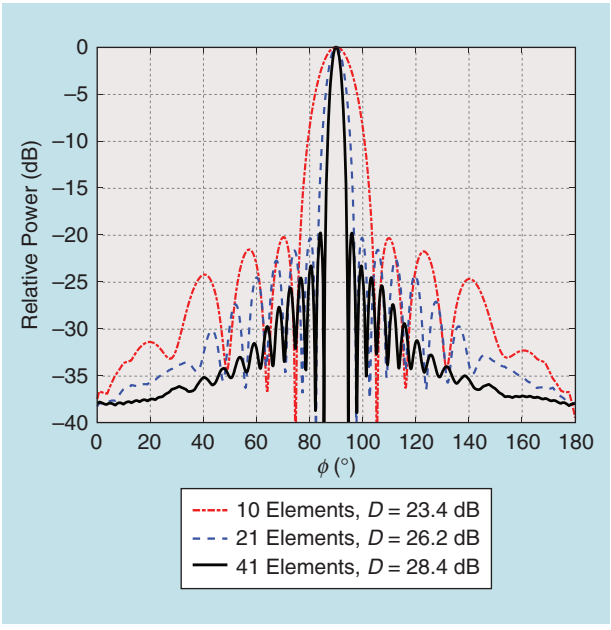


**FIGURE 7.** A comparison of beams formed at 90° azimuth with various numbers of elements at 20 GHz.

and $|F_{\text{norm}}| = |F|/\max\{|F|\}$. The appropriate losses must be included to obtain the gain. For an active receiving array, the SNR is often a more useful measure of performance than gain is [8]. The gains, losses, and noise figures of active devices in the antenna affect the SNR.

## SIMULATION RESULTS

As an example, we consider an array diameter of $a = 0.127$ m and a frequency of 20 GHz. The arc length between elements is 0.0067 m, which corresponds to an angle increment of about 3°. The total number of elements is $N = 119$. If 41 elements are used to form a beam at 90° azimuth, the elements shown in Figure 6(a) are used, and the pattern in Figure 6(b) results when a 20-dB Taylor distribution is applied. The patterns in Figure 7 illustrate how the beamwidth changes with the number of elements used in beamforming. The directivities are $D$ = 23.4 dB, 26.2 dB, and 28.4 dB for 10, 21, and 41 elements, respectively. The rotation of the element normals away from the scan direction due to the curved surface provides a natural amplitude taper that leads to a rapid falloff of the wide-angle sidelobes.

A major advantage of the digital beamforming is that element output data can be shared, and, therefore, multiple simultaneous beams can be formed, as illustrated in Figure 8. Using 21 elements, the beamwidth is approximately 6.2°, so 58 beams would be needed to cover 360° of azimuth, as shown in Figure 9. The elevation pattern is close to the theoretical pattern of an H-plane horn in (6) [7]. The aperture height is 70 mm, resulting in an elevation beamwidth of approximately 15°. This is sufficient for the coverage of surface targets out to the horizon. Mutual coupling effects are identical for all elements due to the circular symmetry. Ideally, the input impedance is the same for all elements.

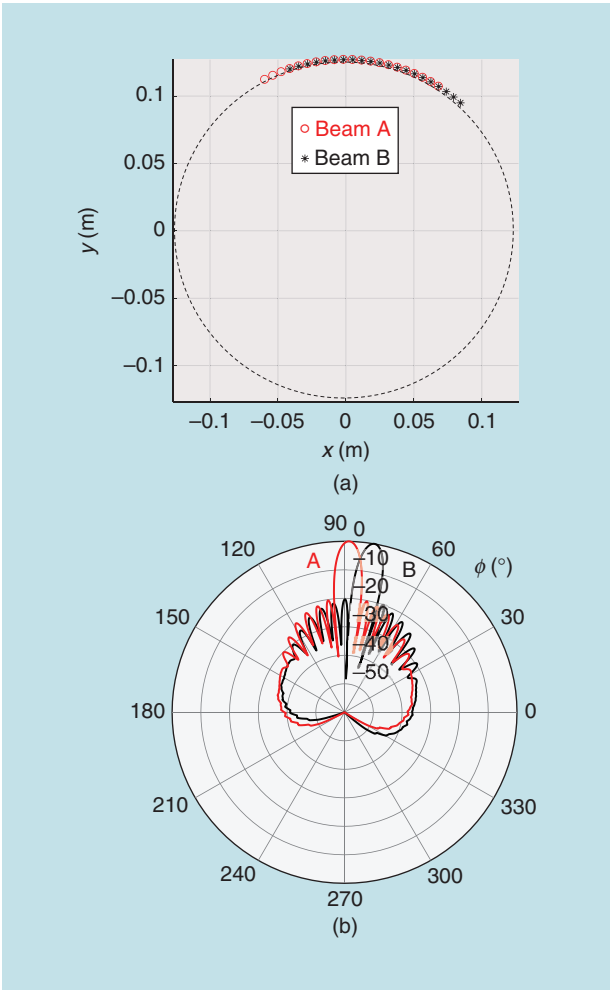


**FIGURE 8.** (a) Elements shared by two adjacent beams and (b) overlapping beam patterns at 20 GHz.

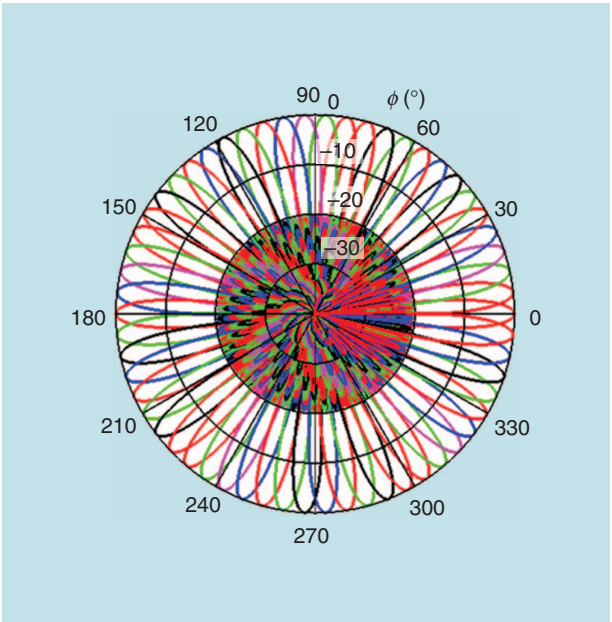


**FIGURE 9.** Overlapping beam patterns for complete azimuth coverage at 20 GHz.

## LEAKAGE CANCELLATION AND CALIBRATION

Both the transmitting and receiving antennas are mounted on the same mast, and the separation distance is limited because both antennas must have a LOS to the horizon. Closely spaced antennas suffer significant transmit–receive leakage. There are a number of propagation or coupling mechanisms that might exist between the two antennas: free-space propagation, near-field coupling, or other propagation modes (such as surface waves along a structure's surface). At long ranges or for low radar cross-section targets, the received signal from the target $s_t(t)$ can be less than the leakage signal $s_l(t)$. The leakage components are changing in time in a manner similar to the time changing in a transmitted waveform. Therefore, these components of leakage are phase coherent and cannot be integrated out.

**A major advantage of the digital beamforming is that element output data can be shared, and, therefore, multiple simultaneous beams can be formed.**

A direct application of the conventional cancellation technique in Figure 10(a) would require a cancellation circuit for each of the array elements. Some hardware reduction can be achieved by exploiting the symmetry of the circular arrays. Theoretically, the leakage signals should be identical at all elements. Therefore, the leakage cancellation signal from a single transmit–receive pair could be distributed to all other pairs. Another possibility is to use an auxiliary antenna to provide a cancellation signal spatially, as originally shown in Figure 1 and detailed in Figure 10(b). Just as for a constrained cancellation channel, a small amount of transmitted signal is coupled off and radiated from the auxiliary antenna. The weights are adjusted to eliminate any received signal from the transmitting array in the absence of a target.

The primary function of the auxiliary antenna is to couple signals as efficiently as possible to the receiving array. The auxiliary antenna operates in the near field of the receiving array, and, therefore, its far-field performance is not a constraint. Several types of antennas are under consideration for the auxiliary, including circular arrays of open-ended waveguides, slots, and dipoles. It is desirable to keep uniform circular symmetry in the auxiliary antenna so that all receiving array elements experience the same coupling environment. The proper delay can be achieved by a combination of free-space delay and circuit delay. An added function of the cancellation signal is calibration and error detection. The phase and amplitude response of each receive channel can be measured and compared to a baseline reference. Compensation for errors can be applied in the digital beamforming and radar processing.

The limitation of coherent cancellation, whether via a circuit or free space, is in the accuracy of the weights. Figure 11 shows a CST Microwave Studio simulation result when cancelling the coupling between two H-plane horns with an open-ended waveguide. The horns are spaced 5.5 in apart, and the cancellation signal has a 1° phase error. The cancellation goes from perfect (infinity in dB) to 35 dB. Phase changes of more than 1° are encountered in practice, just due to temperature changes and frequency drift. Thus, there is

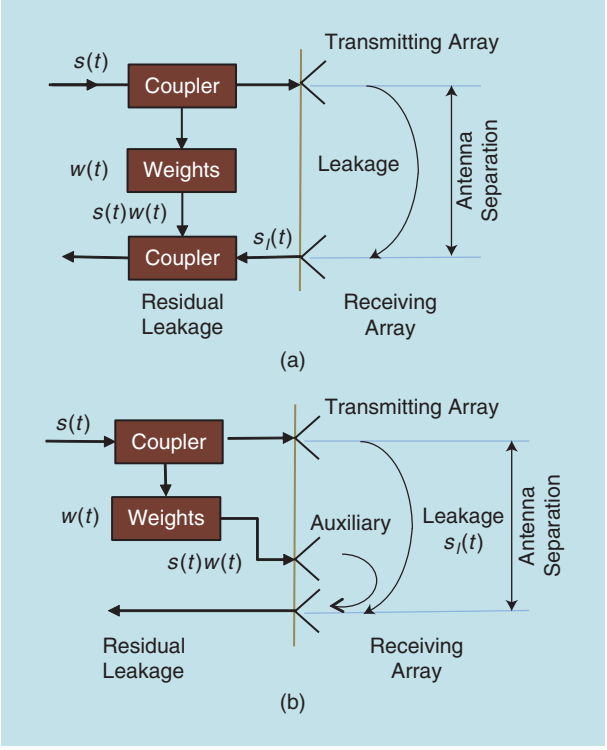


**FIGURE 10.** (a) A coherent leakage cancellation circuit. (b) Coherent leakage cancellation using an auxiliary antenna.

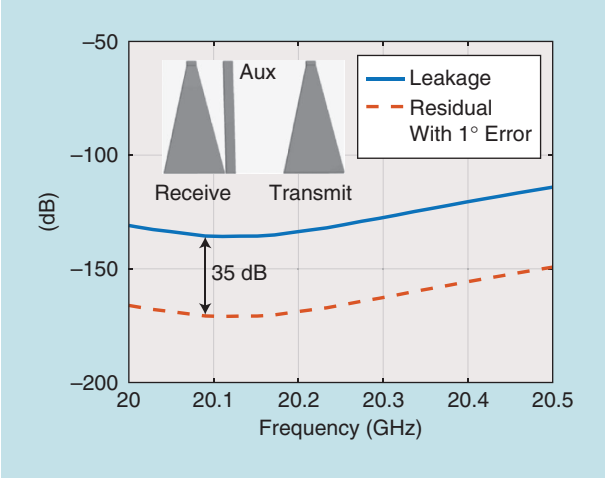


**FIGURE 11.** Residual leakage between two horns when using a cancellation signal from an open-ended waveguide with a 1° phase error.

always some residual leakage remaining after subtraction.

The level of cancellation shown in Figure 11 is still not enough to detect far-out low RCS targets. For radar, an exploitable difference between the target return and leakage signal is the time delay of arrival. Assuming the target is at range $R$, its echo $s_t(t)$ arrives after a time delay of $T_R = 2R/c$, where $c$ is the speed of light [2]. Due to the close-in nature of the leakage, the arrival time of the leakage $T_L$ will be much less. Therefore, if a randomized waveform phase code is used, the leakage and target signals will be uncorrelated. Random radar waveforms have been used previously to lower a radar's probability of intercept [9]. A random noise waveform is transmitted, and the return signal $s_t(t)$ is correlated in the receiver with a delayed replica of the transmitted signal. The correlation provides the processing gain (or time-bandwidth product) for target detection. To an observer without knowledge of the code, the transmitted signal looks like noise.

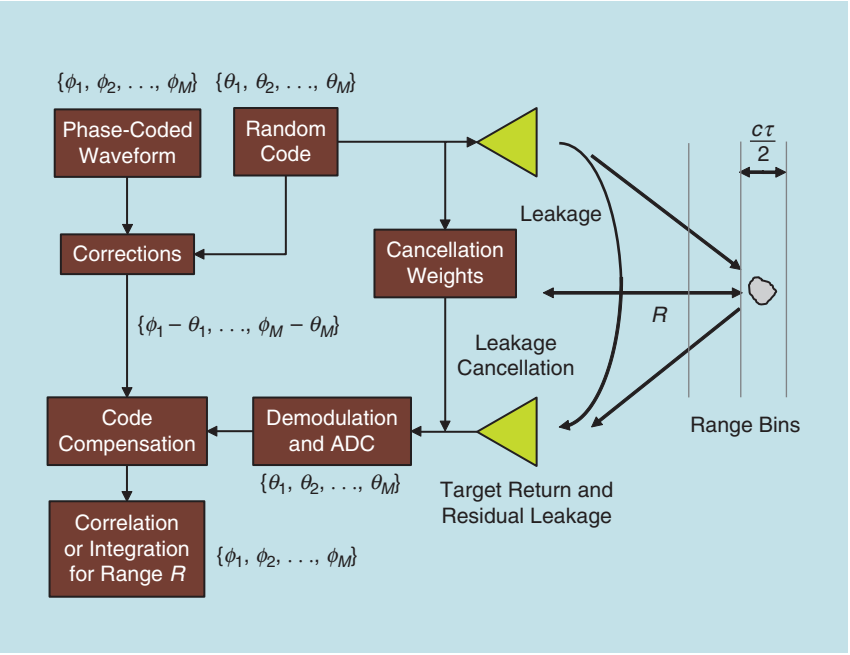


**FIGURE 12.** The application of phase randomization for leakage suppression.

For many radar applications, a random noise waveform is not the preferred one; other phase codes (e.g., Frank, P4, and so on [2]) have more desirable properties. For this radar, we use a robust symmetrical number system–P4 waveform [6] as the base waveform. A random phase waveform is transmitted, and, then, the known random phases are corrected on receive before the radar processing is done. The concept is shown in Figure 12. Let the radar transmitted waveform consist of $M$ random phase subcodes $\{\theta_1, \theta_2, \ldots, \theta_M\}$ of length $\tau$. Also, let the desired base waveform polyphase subcode sequence used for target processing be stored in the receiver.

The returned noise waveform from the target is received, and the random phase of each subcode is detected. The desired (stored) polyphase sequence is obtained from the random phases by applying a phase correction. The required phase rotation for each subcode is obtained from the difference between the random and desired phases for each subcode $\{\phi_1 - \theta_1, \phi_2 - \theta_2, \ldots, \phi_M - \theta_M\}$. After the subcode phase rotation, the resulting (desired) polyphase signal exhibits an ambiguity space with the properties of the base waveform. Because of the differences in time delays, the leakage signal arriving at the same time as the target echo will have different phases than

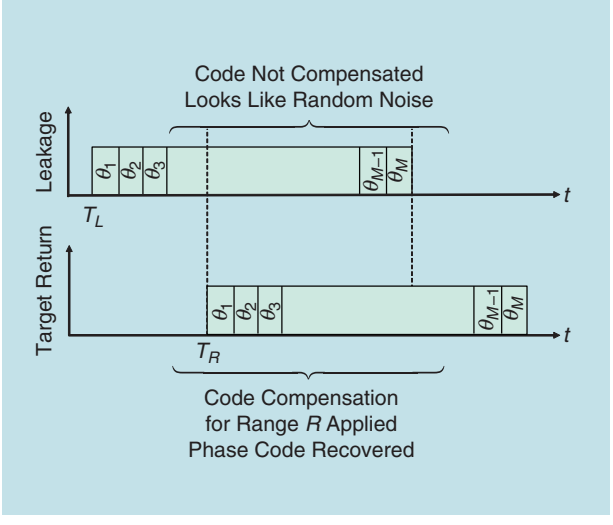


**FIGURE 13.** The time-delay difference between the leakage and target returns for a transmitted phase code.

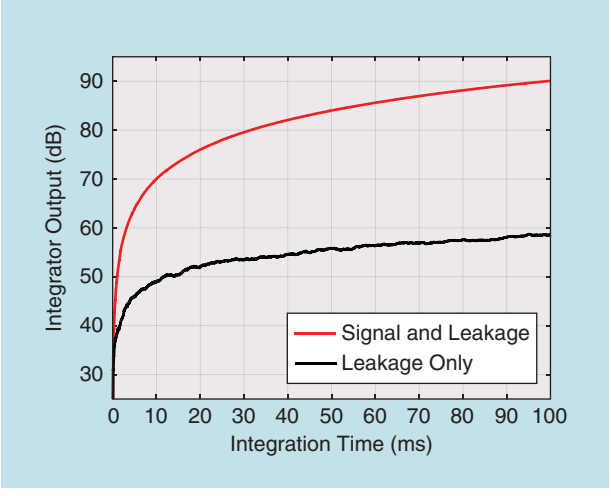


**FIGURE 14.** Integrator output (average for 50 trials) with and without a target present showing a 31.5-dB processing gain after 100 ms.

the target echo does, as illustrated in Figure 13. The proper phase rotations are applied for each range bin, which increases a target's signal, while the leakage appears to be random. Therefore, the signal-to-leakage ratio is increased.

The radar hardware and processing have been simulated using the Keysight Advanced Design System. Simulations have verified that the phase compensation is effective and that the signal-to-leakage ratio can be increased. As an example, consider a waveform with a subcode width of $\tau = 0.1\,\mu s$ and code period of $M = 5 \times 10^5$ subcodes integrated (one complex sample per subcode). The time starts at the range bin in which the target is located. The leakage signal is 0 dB, and the target return is 30 dB lower at the antenna. The curves in Figure 14 are the integrator outputs when a target is present and when no target is present. The average of 50 trials is shown for an integration time of 100 ms. Because of the pseudorandom nature of the phase code, the integrated output of the leakage does not experience the same improvement that the signal does. As shown in Figure 14, the signal-to-leakage ratio at the output is 31.5 dB after 100 ms. This represents a processing gain for the target of approximately 61.5 dB. A further improvement can be realized with a longer integration time.

## SUMMARY AND CONCLUSIONS

In this article, we described a bistatic radar that uses an omnidirectional transmitting array with analog beamforming and a receiving array architecture with digitally formed simultaneous overlapping beams for search and track. The received signals are downconverted to an IF where they are digitized and processed. For the present design, the radar bandwidth is relatively narrow, but the operating band can be shifted, and it is limited by the bandwidth of the antenna elements. The capability to form simultaneous beams allows for long integration times that can provide processing gain to increase the SNR.

The method of random phase coding of the radar's transmitted signal for the purpose of transmit–receive leakage suppression was also described. A random phase code is transmitted, and the target's received random phases are transformed based on the underlying desired phase code that is used in the target processing. At every instant of time, the transmitted and received phases are known precisely. This allows signal processing to be performed for any desired phase code. In this sense, there is a similarity to digital beamforming, where the incident wave phase is known precisely, and, thus, any desired array weighting can be applied.

In the integration, the leakage signal appears as noise, and significant target signal-to-leakage improvement can be achieved. Using this technique, there is a minimum range corresponding to one subpulse length $\tau$ time delay, inside of which the method cannot be applied. Both of these capabilities are made possible by the digital architecture of the radar system and array. The combination of analog and digital design achieves a performance and operational flexibility that would be difficult to obtain with a purely analog or digital architecture.

**In the integration, the leakage signal appears as noise, and significant target signal-to-leakage improvement can be achieved.**

## ACKNOWLEDGMENT

This work was supported in part by the Office of Naval Research.

## AUTHOR INFORMATION

***David C. Jenn*** (jenn@nps.edu) is a professor with the Department of Electrical and Computer Engineering at the Naval Postgraduate School, Monterey, California. His research interests include antennas and radar cross section. He is a Senior Member of the IEEE.

***Phillip E. Pace*** (pepace@nps.edu) is a professor with the Department of Electrical and Computer Engineering at the Naval Postgraduate School, Monterey, California. His research interests include radar and electronic warfare. He is a Fellow of the IEEE.

***Ric A. Romero*** (rmromero@nps.edu) is an associate professor with the Department of Electrical and Computer Engineering at the Naval Postgraduate School, Monterey, California. His research interests include radar, detection, estimation, and communications. He is a Senior Member of the IEEE.

## REFERENCES

[1] P. E. Pace, *Detecting and Classifying Low Probability of Intercept Radar*, 2nd ed. Norwood, MA: Artech House, 2009.

[2] M. Skolnik, *Introduction to Radar Systems*, 3rd ed. New York: McGraw-Hill, 2001.

[3] A. Stove, "Linear FMCW radar techniques," *IEE Proc. F*, vol. 139, no. 5, pp. 343–350, 1992. [Online]. Available: https://digital-library.theiet.org/content/journals/10.1049/ip-f-2.1992.0048

[4] K. Lin, Y. Wang, C. Pao, and Y. Shih, "A Ka-band FMCW radar front-end with adaptive leakage cancellation," *IEEE Trans. Microw. Theory and Techn.*, vol. 54, no. 12, pp. 4041–4048, 2006. [Online]. Available: https://ieeexplore.ieee.org/document/4020466

[5] K. Cooper and R. Dengler, "Residual phase noise and transmit/receive isolation in a submillimeter-wave FMCW radar," in *Proc. 2014 IEEE MTT-S Int. Microwave Symp.* doi: 10.1109/MWSYM.2014.6848268.

[6] P. E. Pace, S. Teich, O. Brooks, D. Jenn, and R. Romero, "Extended detection range using a polyphase CW modulation with an efficient number theoretic correlation process," in *Proc. 2017 IEEE Radar Conf.*, pp. 1669–1674.

[7] W. Stutzman and G. Thiele, *Antenna Theory and Design*, 3rd ed. Hoboken, NJ: Wiley, 2012.

[8] J. J. Lee, "G/T and noise figure of active array antennas," *IEEE Trans. Antennas Propag.*, vol. 41, no. 2, pp. 241–244, 1993. [Online]. Available: https://ieeexplore.ieee.org/document/214619

[9] Y. Zhang and R. Narayanan, "Design considerations for a real-time random-noise tracking radar," *IEEE Trans. Aerosp. Electron. Syst.*, vol. 40, no. 2, pp. 434–444, 2004.